VOLTAGE OSCILLATIONS IN THE BARNACLE GIANT MUSCLE FIBER

CATHERINE MORRIS AND HAROLD LECAR, *Laboratory of Biophysics, National Institute of Neurological and Communicative Disorders and Stroke, National Institutes of Health, Bethesda, Maryland 20205*

ABSTRACT Barnacle muscle fibers subjected to constant current stimulation produce a variety of types of oscillatory behavior when the internal medium contains the Ca^{++} chelator EGTA. Oscillations are abolished if Ca^{++} is removed from the external medium, or if the K^+ conductance is blocked. Available voltage-clamp data indicate that the cell's active conductance systems are exceptionally simple. Given the complexity of barnacle fiber voltage behavior, this seems paradoxical. This paper presents an analysis of the possible modes of behavior available to a system of two noninactivating conductance mechanisms, and indicates a good correspondence to the types of behavior exhibited by barnacle fiber. The differential equations of a simple equivalent circuit for the fiber are dealt with by means of some of the mathematical techniques of nonlinear mechanics. General features of the system are (*a*) a propensity to produce damped or sustained oscillations over a rather broad parameter range, and (*b*) considerable latitude in the shape of the oscillatory potentials. It is concluded that for cells subject to changeable parameters (either from cell to cell or with time during cellular activity), a system dominated by two noninactivating conductances can exhibit varied oscillatory and bistable behavior.

INTRODUCTION

Voltage-clamp studies of the barnacle muscle (Keynes et al., 1973; Hagiwara et al., 1969; Hagiwara et al., 1974; Murayama and Lakshminarayanaiah, 1977; Beirao and Lakshminarayanaiah, 1979) indicate that the fiber possesses a simple conductance system consisting of voltage dependent Ca^{++} and K^+ channels, neither of which inactivates appreciably. Current-clamp studies, however, show complicated oscillatory voltage behavior (Hagiwara and Nakajima, 1966; Murayama and Lakshminarayanaiah, 1977). In this paper we ask whether a system of two noninactivating conductances can, in fact, account for such phenomena. A mathematical study shows that this simple system can predict much of the barnacle fiber behavior, although the simplest model fails to explain some areas of behavior.

Of the two species of ion conductances in barnacle muscle (voltage- and time-dependent), neither shows fast inactivation, although accumulation of permeating ions produces time-dependent reduction of K^+ currents (Keynes et al., 1973) and may also account for the slow but variable decay of Ca^{++} channel currents. Two noninactivating conductances would constitute an unusually simple conductance apparatus, compared with other crustaceans (cf. Mounier and Vassort, 1975; Hencek and Zachar, 1977). There is preliminary evidence for a Ca^{++}-activated g_K in the barnacle fiber (Murayama and Lakshminarayanaiah, 1977). In our analysis this process would not enter into consideration of the primary oscillation, but it might effect slow modulations to produce "bursting" phenomena similar to those modelled for

Aplysia neuron (Plant and Kim, 1976; Plant, 1976). Since our current clamp records were obtained from EGTA-perfused fibers, any Ca^{++}-dependent slow processes would necessarily be depressed. We do, however, indicate how Ca^{++} accumulation at the inner surface of the membrane may act as a very slow "inactivation" process.

With I_K and I_{Ca} dominating the membrane, it would be reasonable to anticipate a limited repertoire of voltage behavior in barnacle fibers. Under physiological conditions this is indeed the case: the barnacle fiber responds to nerve stimulation like other crustaceans, with graded depolarizations. But EGTA-perfused fibers subjected to constant current stimulation exhibit a variety of complicated voltage responses. One is compelled to ask whether the two noninactivating conductances would be sufficient to produce voltage oscillations as variable in character as those illustrated in the literature (cf. Hagiwara and Nakajima, 1966; Murayama and Lakshiminarayanaiah, 1977). Other factors, such as failure of radial space clamp (caused by membrane invaginations), ion accumulation, slow inactivation, inhomogeneous distribution of channel types, and further species of conductances, could all lend additional complexity to the system and perhaps even cause additional oscillations.

In this paper we consider the voltage oscillations induced under current clamp, and explore the possibility that they are produced by nothing more than two noninactivating conductances distributed homogeneously in a well space-clamped membrane. The observed behavior is compared with that predicted from a simple theoretical model. Although the model will be seen to give a reasonably good quantitative account of the current-clamp data, accurate fitting of the data for a limited set of conditions is not our main concern, since the extant voltage-clamp data are variable (cf. Keynes et al., 1973; Hagiwara et al., 1974). Rather, we study the range of behavior available to an excitable system of two nonlinear, noninactivating conductances, showing how the system predicts not only oscillations, but also pronounced qualitative variations in the character of the oscillations for different sets of parameters. Although this does not, of course, preclude involvement of other factors, it suggests that they have only a modulating influence, and are not fundamental to the oscillations.

LIST OF ABBREVIATIONS OF MODEL PARAMETERS

I = applied current ($\mu A/cm^2$)
I_L, I_{Ca}, I_K = leak, Ca^{++}, and K^+ currents, respectively ($\mu A/cm^2$)
g_L, g_{Ca}, g_K = maximum or instantaneous conductance values for leak, Ca^{++}, and K^+ pathways, respectively ($mmho/cm^2$)
g^*_{Ca} = conductance constant for nonlinear I_{Ca} ($mmho/cm^2$)
V = membrane potential (mV)
V_L, V_{Ca}, V_K = equilibrium potential corresponding to leak, Ca^{++}, and K^+ conductances, respectively (mV)
M = fraction of open Ca^{++} channels
N = fraction of open K^+ channels
$M_\infty(V)$, $N_\infty(V)$ = fraction of open Ca^{++} and K^+ channels, at steady state
$\lambda_M(V)$, $\lambda_N(V)$ = rate constant for opening of Ca^{++} and K^+ channels (s^{-1})
λ_M, λ_N = maximum rate constants for Ca^{++} and K^+ channel opening (s^{-1})
$V1$ = potential at which $M_\infty = 0.5$ (mV)
$V2$ = reciprocal of slope of voltage dependence of M_∞ (mV)
$V3$ = potential at which $N_\infty = 0.5$ (mV)
$V4$ = reciprocal of slope of voltage dependence of N_∞ (mV)

$[Ca^{++}]_i$, $[Ca^{++}]_o$ = internal and external Ca^{++} concentration (mM)
K = accumulation-layer constant (cm^{-1})
F = Faraday constant
C = membrane capacitance ($\mu F/cm^2$)

METHODS

Large specimens of the barnacle *Balanus nubilus* (Pacific Bio-Marine Laboratories Inc., Venice, Calif.) were used. The barnacle was sawed into lateral halves, and the *depressor scutorum rostralis* muscles were carefully exposed. Individual fibers were dissected, the incision starting from the tendon. The other end of the muscle was cut close to its attachment on the shell and ligatured. Isolated fibers were either used immediately or kept for up to 30 min in standard artifical seawater (ASW; see below) before use. Experiments were carried out at room temperature of ~22°C.

The muscle chamber, internal and external electrodes, internal perfusion system and current clamping system were essentially similar to those described by Keynes et al. (1973).

The composition of the normal internal solution was: K acetate (180 mM), glucose (600 mM), Tris OH (12.5 mM), and EGTA (2.5 mM). For some experiments the internal solution consisted of Cs acetate (180 mM), TEA chloride (60 mM), glucose (485 mM), Tris OH (12.5 mM), and EGTA (2.5 mM). The external solutions were either normal ASW (385 mM NaCl, 10 mM KCl, 10 mM $CaCl_2$, 50 mM $MgCl_2$, and 10 mM TES), high-Ca^{++} ASW (325 mM NaCl, 10 mM KCl, 100 mM $CaCl_2$, and 10 mM TES, or Ca^{++}-free ASW as normal ASW except $CaCl_2$ substituted by $MgCl_2$).

Most of the results are presented in conjunction with theoretical computations of voltage oscillations. The differential equation systems were integrated using the MLAB program developed at National Institutes of Health (NIH) (Knott, 1979). This program employs the Geary-Nordsieck algorithm for numerical integration, which is adequate for our problem. Much of the analysis makes use of methods of nonlinear mechanics, and various analytical results are given in the text in order to gain insight into the requirements for oscillation.

The Model

In accord with the voltage-clamp experiments of Keynes et al. (1973), the model is assigned two independent voltage-dependent conductances, g_K and g_{Ca}, each having a sigmoid voltage dependence. The relaxation times with which these conductances approach new values after voltage changes are given as bell-shaped functions of voltage. We shall assume for simplicity that the relaxation kinetics are first order, since precise kinetics are not essential for the description of all excitation effects (cf. Lecar and Nossal, 1971; FitzHugh, 1961). In general we have used linear relations for the instantaneous current-voltage curves through open-channels. Although our own experiments on the instantaneous Ca^{++} current in barnacle muscle (unpublished data) show departures from linearity, under situations of high permeable-ion gradient, in all but one instance we stick for the sake of simplicity to the linear driving force approximation. The exception occurs when we look at the Ca^{++} conductance system in isolation from g_K, for under these circumstances there is no countering force to keep the system in the nearly linear region.

Fig. 1 shows the equivalent circuit hypothesized for a space-clamped patch of sarcolemma membrane. The equations describing the membrane behavior are:

$$\begin{aligned} I &= C\dot{V} + g_L(V_L) + g_{Ca}M(V - V_{Ca}) + g_K N(V - V_K) \\ \dot{M} &= \lambda_M(V)\,[M_\infty(V) - M] \\ \dot{N} &= \lambda_N(V)\,[N_\infty(V) - N]. \end{aligned} \tag{1}$$

The parameters and variables are defined in the list of abbreviations. The variables M and N are

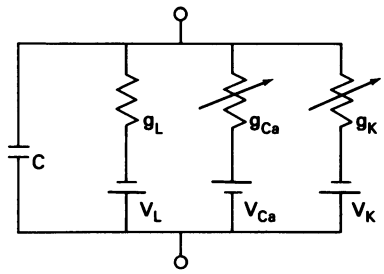

FIGURE 1 Equivalent circuit for a patch of space-clamped barnacle sarcolemma.

analogous to the Hodgkin-Huxley (1952) "m" and "n" parameters. M and N are the fraction of channels open at any given time and, by rather elementary statistical arguments, are given the forms (e.g., Lecar et al., 1975; Ehrenstein and Lecar, 1977):

$$\begin{aligned} M_\infty(V) &= 1/2\,\{1 + \tanh\,[(V - V_1)/V_2]\} \\ \lambda_M(V) &= \overline{\lambda_M}\cosh\,([V - V_1]/2V_2) \\ N_\infty(V) &= 1/2\,\{1 + \tanh\,[(V - V_3)/V_4]\} \\ \lambda_N(V) &= \overline{\lambda_N}\cosh\,([V - V_3]/2V_4). \end{aligned} \tag{2}$$

Eqs. 1 and 2 represent a third-order nonlinear system of the Hodgkin-Huxley form, which we shall use to explain the excitation behavior of the barnacle muscle. Values for the parameters were drawn from the voltage-clamp literature or from our own voltage-clamp data. In many cases we shall focus on the way in which the character of the solutions changes as the parameters are made to vary.

RESULTS

Experimental Observations

Voltage behavior of current-clamped fibers was observed under three different conditions: with Ca^{++}-free external solution (to minimize g_{Ca}), with Cs/TEA-containing internal perfusion solution (to minimize g_K), and with solutions that optimize both g_K and g_{Ca}.

K^+ Conductance

In Ca^{++}-free solutions fibers produce no voltage oscillations. The membrane response to small stimuli is not discernably different from a passive RC circuit, but as the stimuli increase, a small active response is seen (Fig. 2*a*); instead of maintaining a voltage that would be dominated by the drop across the leakage resistance, the membrane partially repolarizes, leaving a small peak where the purely RC-response is truncated. At the end of the stimulus the voltage (which has usually slightly depolarized again) returns almost exponentially to rest. The straightforward interpretation is that the larger stimuli activate a nonlinear K^+ conductance, thereby producing an outward, hyperpolarizing current. The subsequent slow polarization of the K^+ plateau is probably due to K^+ accumulation during the prolonged stimulus (Keynes et al., 1973) and/or to a small residual Ca^{++} current, but not to g_K inactivation.

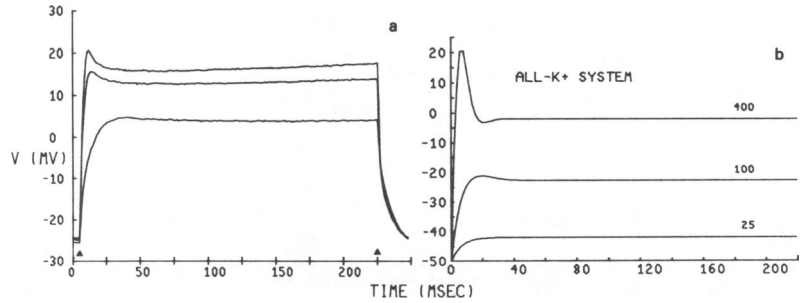

FIGURE 2 Plateau potentials of the K^+ system. (*a*) Voltage responses (in millivolts) of a fiber to increasing current stimulus (480, 960, and 1200 $\mu A/cm^2$). External saline: Ca^{++}-free ASW. Internal saline: K^+ perfusate. In this and subsequent records, the duration (in milliseconds) of the current stimulus is indicated by arrowheads. (*b*) Computed voltage response of model to increasing currents. These curves represent numerical solutions to Eq. 3 for $I = 25$, 100, and 400. Other parameters were as follows: $g_{Ca} = 0$, $g_K = 8$, $g_L = 3$, $V_K = -70$, $V_L = -50$, $\bar{\lambda}_N = 1/15$, $C = 20$, $V3 = -1.0$, $V4 = 14.5$. Initial conditions: $V(0) = -50$, $N(0) = N_\infty(-50)$. The value for g_L was set at 3 instead of 2 to simulate roughly the increased leak frequently encountered in Ca^{++}-free solutions.

Ca^{++} Conductance

The behavior of g_K-blocked fibers is somewhat more complex. Again, no oscillations are observed, and very small stimuli produce simple *RC*-like responses. With increasing stimuli, however, a threshold is reached and bistability in the membrane voltage becomes evident. Beyond a threshold (~ -17 mV) the membrane voltage shoots rapidly to about $+20$ mV and remains in a depolarized state with a slow repolarizing droop. This is a "Ca^{++} plateau action potential" (Fig. 3*a*, top trace). When the stimulus pulse ends, the fiber does not return to rest, but simply undergoes a small voltage drop caused by the removal of the stimulating current. Between hundreds of milliseconds and several seconds later, as the plateau voltage continues to decline, the voltage does reach a threshold and falls precipitously to rest (Fig. 3*c*). The threshold for returning to rest occurs at a more depolarized voltage ($\sim$ 0 mV) than for activation.

The plateau action potential is readily interpreted as indicating that the only operative conductance system of significance (when g_K is blocked) is a nonlinear g_{Ca}. Threshold behavior would result from the negative resistance provided by the inward, depolarizing I_{Ca}; bistability would follow from lack of voltage-sensitive inactivation in the negative resistance element.

Oscillations: K^+ and Ca^{++} Conductances Together

The voltage behavior of the current-clamped fiber when either g_K or g_{Ca} is minimized is relatively simple and predictable; essentially, stimulation results in one of two types of plateaus. One might anticipate that when both conductances are recruited simultaneously, a voltage plateau intermediate between those for all K^+ and all Ca^{++} would result. This is not, however, the case; the voltage behavior, over a wide range of current stimulus, is oscillatory.

Small stimuli produce small, essentially passive depolarizations, but once a threshold voltage (which is in the same range as the all-Ca^{++} threshold) is reached, oscillations appear.

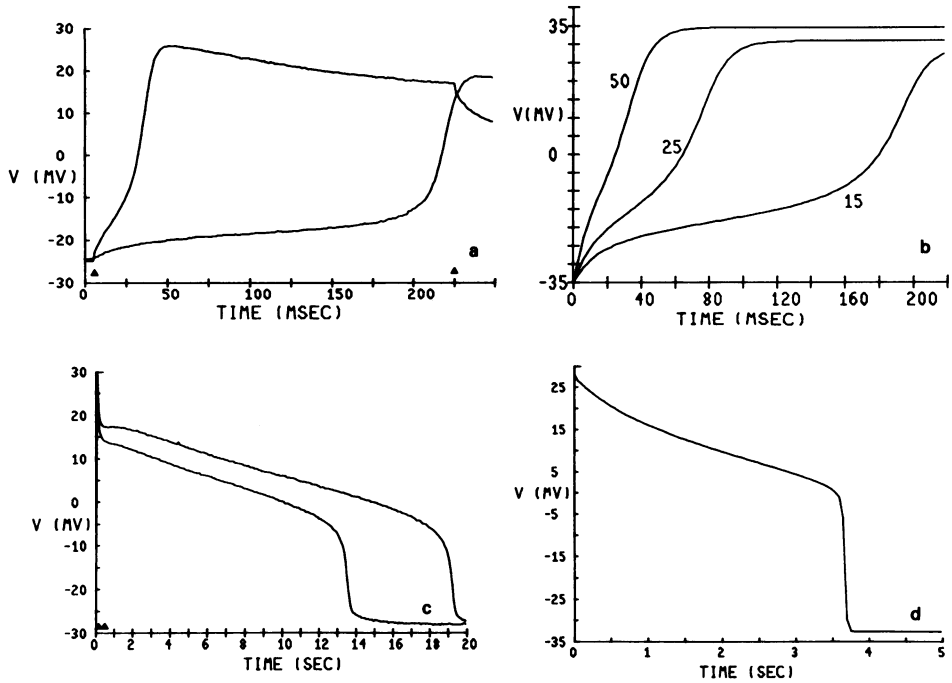

FIGURE 3 Plateau potentials of the all-Ca^{++} system. (*a*) Voltage responses (in millivolts) of a fiber to two values of current stimulus, 60 $\mu A/cm^2$ (lower trace) and 240 $\mu A/cm^2$ (upper trace). Note that for the smaller current the voltage reaches its plateau value after the stimulus is over. Time is expressed in milliseconds. External saline: high-Ca^{++} ASW (100 mM Ca^{++}). Internal saline: Cs/TEA/EGTA perfusate. (*b*) Voltage response (mV) of the model (nonlinear driving force) to increasing currents. These curves represent numerical solutions to eq. 3 and 7, for I = 15, 25, and 50. Other parameters were as follows: $g_K = 0, g_{Ca} = 40, g_L = 2, [Ca^{++}]_i = 0, [Ca^{++}]_o = 100, V_L = -35, \bar{\lambda}_M = 0.1, C = 20, V1 = 10, V2 = 15$. Initial conditions $V(0) = -35, M(0) = M_\infty(-35)$. Time is expressed in milliseconds. (*c*) Responses of a fiber to two subsequent current stimuli (360 μA) 1 min apart (upper trace first). Duration of the stimulus is 100 ms, so that these records emphasize the poststimulus part of the response. These represent particularly long plateau action potentials, but are typical in shape. Voltage, mV; Time, s. (*d*) Poststimulus voltage response of the model with an accumulation term. This curve represents a solution to Eq. 8 for $I = 0$. Other parameters were as follows: $g_K = 0, g_{Ca} = 40, g_L = 2, [Ca^{++}]_o = 100, V_L = -35, V1 = 10, V2 = 15, C = 20, K = -10^{-4}$. Initial conditions $V(0) = +28, [Ca^{++}]_i(0) = 0.001$. Voltage, mV; time, s.

Oscillations of barnacle muscle fibers are decidedly not stereotyped (see also Hagiwara and Nakajima, 1966; Murayama and Lakshminarayanaiah, 1977); they are variable and sometimes complex. Depending on experimental parameters such as leakage or Ca^{++} conductance, the oscillations can either be damped or continuous. Usually, but not always, oscillations cease at the end of the stimulus and the fiber returns to rest. Fig. 4*a* shows a sequence of damped oscillations for various values of applied current. Although the amplitude and frequency of the oscillations are dependent on stimulus strength, increasing the stimulus does not produce a monotonic change in oscillation amplitude and frequency. Eventually, as I increases, the voltage excursions decrease and the rate of damping of the oscillations increases.

Factors other than current strength also influence the character of the oscillations. The external calcium ion concentration is particularly influential. Fibers that show little or no

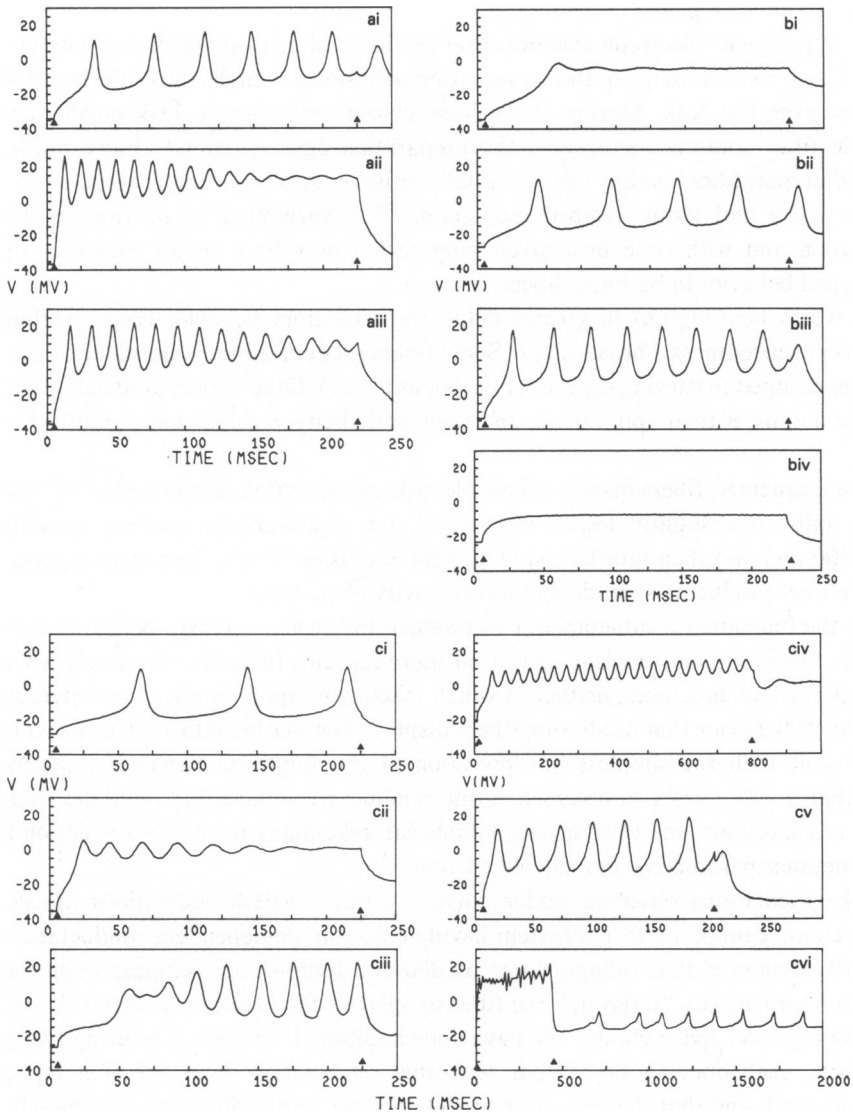

FIGURE 4 Voltage oscillations in fibers with Ca^{++} and K^+ conductances. External saline: either ASW (*ai*, *aii*, *aiii*, *bi*, *biii*, *cii*), Ca^{++}-free ASW (*biv*), or, in all others, high Ca^{++} ASW. Internal saline: K^+ perfusate. Voltage, mV; time, ms. (*a*) Voltage responses of a fiber to varying current stimulus. Current from top to bottom: 180, 540, and 900 μA. (*b*) Effect of varying $[Ca^{++}]_o$. Current stimulus, 240 μA. *i*, *ii*, and *iii*, *iv* are from two different fibers. In *i* and *ii*, $[Ca^{++}]_o$ is increased from 10 mM (*i*) to 100 mM (*ii*). In *iii* and *iv* it is decreased from 10 mM (*i*) to 0 mM (*iv*). The contrast between *i* and *iii* also illustrates how variable the oscillatory response can be from fiber to fiber. Trace *iv* illustrates the *RC* response of the fiber in 0 mM Ca^{++}. (*c*) Variety of oscillatory characteristics. Current stimuli are 180, 600, 180, 360, 960, and 600 μA from *i* through *vi*.

oscillations in normal saline (10 mM Ca^{++}) usually will oscillate when 100 mM Ca^{++} is substituted. Fibers which oscillate in normal saline change their mode of oscillation in 100 mM Ca^{++} saline (Fig. 4*b*).

The "piggyback" electrode assembly that perfuses saline through the cell interior produces variable degrees of damage to the invaginating membrane, which leads to individual variation in the nonspecific leak. During the voltage-clamp experiments, leak conductance of the barnacle fiber tends to increase as the preparation ages (personal observation). Current-clamped preparations, as they age, eventually either cease oscillating in response to stimuli or produce more and more damped oscillations. The variability of g_L from preparation to preparation and with time in a given preparation may be a major factor in the lack of stereotyped behavior in barnacle fibers.

It is worth pointing out in greater detail the oscillatory behavior types exhibited by the fiber, which encompass a broad range. Some fibers produce almost sinusoidal oscillations, and these are damped to varying degrees (Fig. 4*cii* and 4*civ*). Other fibers produce trains of spikes, with the details of their spike shape and their periodicity varying considerably (Fig. 4*ci* and 4*civ*).

Quite frequently, fibers display a bistable type of oscillation: at the end of the stimulus the voltage falls to a slightly lower mean level, but continues to oscillate (usually for not >100–200 ms) and then falls to rest (Fig. 4*ai*). Occasionally this bistability appears chaotic, with the fiber producing sporadic bursts of activity (Fig. 4*cvi*).

How the individual conductances can produce the type of plateau behavior shown by the barnacle fiber seems fairly clear. It is a bit more difficult to decide intuitively whether these two nonlinear conductances, neither of which inactivates appreciably, could interact to create the array of behavior that oscillating fibers display. The mathematical analysis which follows is consistent with the simplest interpretation of the single-conductance experiments, and shows that a system of two noninactivating nonlinear conductances oscillates under a wide variety of conditions, and that the oscillations can take many forms, dependent on the values of conductance parameters and applied current.

Unlike oscillations observed under current clamp, current oscillations observed under voltage clamp cannot occur in a system having only voltage-dependent conductances. Keynes et al. (1973) showed that voltage-clamp oscillations diminish or disappear when radial space clamp is improved (by "inflating" the fiber to open up the membrane clefts). In our analysis we assume perfect space clamp. We have done additional computations using two patches of membrane, each obeying Eq. 1, but separated by a series resistance. For current-clamp conditions we found that the two-patch model does not give oscillations qualitatively different from the space-clamped model, although the detailed quantitative solutions change. For voltage-clamp conditions, on the other hand, there is an optimum range of cleft resistance for which the cleft membrane shows current oscillations even though the surface membrane is under potential control. The oscillations seen under voltage clamp may therefore be induced as approximate current-clamp oscillations of the cleft membrane when departure from radial space clamp is taken into account. The two-patch computation simulated the voltage-clamp oscillations and also their diminution (by varying the cleft-resistance parameters). Thus, it seems reasonable to conjecture that, because of the complicated membrane geometry, the

system responsible for voltage oscillations under current clamp can also account for current oscillations under voltage clamp under conditions that are, by definition, imperfect.

ANALYSIS

To explore the contribution of the components of the overall conductance system, we shall examine in turn the behavior of each of the two nonlinear conductances operating in isolation from the other. The behavior of the two nonlinear conductances acting in concert will be examined afterward. This should demonstrate how the interaction of the two nonlinear conductances produces novel behavior.

Responses of System with a Single Voltage-dependent Conductance

Consider a system in which either the Ca^{++} or the K^+ system is working in isolation. Figs. 2*b* and 3*c* show that the all-Ca^{++} system has bistable responses and a characteristic threshold, whereas the all-K^+ system exhibits a graded response with a transient peak followed by a decay to a voltage plateau.

Let us generalize and write the equation of a single-conductance system as:

$$\begin{aligned} I &= C\dot{V} + g_L(V - V_L) + g_i\mu\,(V - V_i) \\ \dot{\mu} &= \lambda\,(V)\,[\mu_\infty(V) - \mu] \end{aligned} \tag{3}$$

Here μ can be either M or N, and the subscript i stands either for Ca or K. The main qualitative difference between the two cases is whether V_i is less than or greater than V_L. For these systems, $V_{Ca} > V_L$ and $V_K < V_L$. Other parameters describing the voltage-dependent conductances are not very different for the two systems. Let us study the behavior of Eqs. 3 in the V, μ-phase plane. We can write the equations for the nullclines (that is, the $\dot{V} = 0$ and $\dot{\mu} = 0$ isoclines) explicitly as

$$(\dot{V} = 0 \text{ nullcline})\ V(\mu) = (I + g_L V_L + g_i\mu V_i)/(g_L + g_i\mu), \tag{4a}$$

$$(\mu = 0 \text{ nullcline})\ \mu(V) = \mu_\infty(V). \tag{4b}$$

Eq. 4 shows that the $\dot{V} = 0$ nullcline is a bilinear function of μ, which varies between the values

$$V(0) = (I + g_L V_L)\ /\ g_L,$$

and

$$V(1) = (I + g_L V_L + g_i V_i)\ /\ (g_L + g_i). \tag{5}$$

Fig. 5 shows nullclines for typical all-K^+ and all-Ca^{++} conditions, illustrating the qualitative difference between the two cases. When $V_i < V_L$ (all-K^+) there can be only one singular point, whereas when $V_i > V_L$ (all-Ca^{++}) there can be as many as three singular points. The $\dot{\mu} = 0$ nullcline is approximately the same in both cases, with slight shifts along the voltage axis and slight differences in steepness.

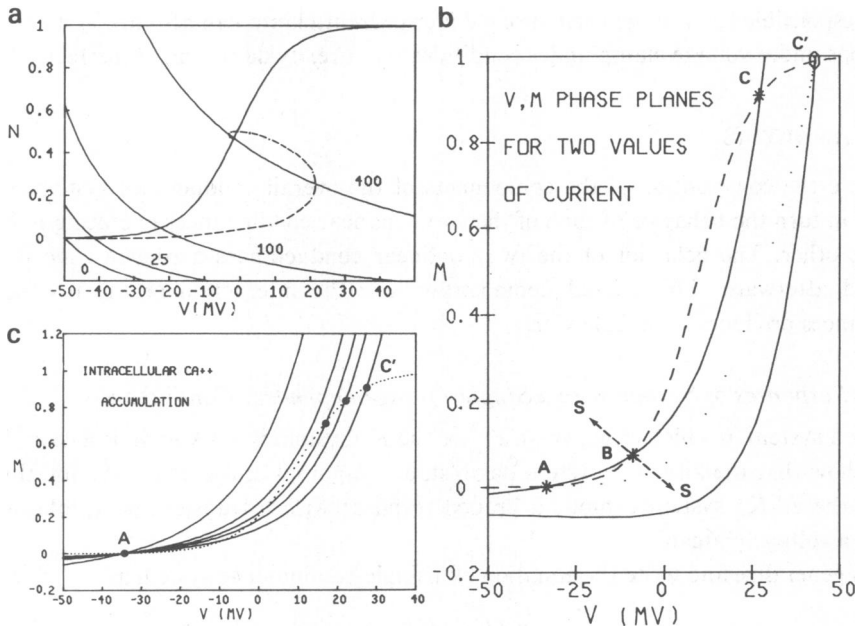

FIGURE 5 (*a*) *V,N* phase plane for all-K^+ system. Dotted curve shows a typical phase trajectory when applied current is switched from 0 to 400. $\dot{V} = 0$ nullclines are shown for various values of applied current, *I*. The intersection of the $N = 0$ and $\dot{V} = 0$ nullcline for each value of current is the sole singular point for the all-K^+ system for that set of parameters and is always a stable node. Parameters used are $g_L = 3$, $g_{Ca} = 0$, $g_K = 8$, $V_L = 50$, $V_K = -70$, $V3 = -1.0$, $V4 = 14.5$, $\bar{\lambda}_N = 1/15$, $C = 20$. Voltage; V is expressed in millivolts. (*b*) *V, M* phase plane for all-Ca^{++} system. Parameters are those given for Fig. 3*b* except for values of *I*. Dotted curve is the phase trajectory when *I* is switched from 0 to 100. The dashed curve is the $\dot{M} = 0$ isocline. The two solid curves are the $\dot{V} = 0$ isoclines for $I = 0$ and $I = 100$. The $I = 0$ nullclines intersect at three points, *A*, *B*, and *C*. The points *A* and *C* are stable nodes, whereas *B* is a saddle point. The pattern of the three singular points leads to bistable behavior as explained in the text. When *I* is switched to 100 there is only one singular point, *C*; this stable node determines the plateau voltage. The line S–S represents the threshold separatrix, sketched in approximately. (*c*) The effects of intracellular Ca^{++} accumulation shown on the *V, M* phase plane. The dotted line is the $\dot{M} = 0$ nullcline and the series of solid lines are $\dot{V} = 0$ nullclines for increasing degrees of Ca accumulation (from right to left, g_{Ca}^* is decreased arbitrarily as follows: 40, 30, 25, 20, 10. Concurrently $[Ca^{++}]_i$ is increased as follows: 0.001, 0.1, 0.5, 1.0, 10. Other parameters are as for Fig. 3*b*, but with $I = 0$. Ca^{++} accumulation causes the $\dot{V} = 0$ nullcline to shift to the left, ultimately causing the stable point *C* to disappear, the system reverting to monostable behavior about the resting point *A*.

The computer response of the all-Ca^{++} system, with a linear instantaneous Ca^{++} *I–V* relation, gives an unrealistically high voltage plateau. The problem is that, although the linear *I–V* relation implies some outward current, the experiments were done with close to zero internal Ca^{++}. Thus, a better quantitative fit to the plateau is obtained by modifying the driving force term in Eq. 3. It is more accurate to write:

$$I_{Ca} = -\overset{*}{g}_{Ca} MR(V, [Ca^{++}]_i, [Ca^{++}]_o), \tag{6}$$

where, in general, the conductance $\overset{*}{g}_{Ca}$ would be a function of the permeating ion concentration, but can be obtained by empirical fit to the instantaneous Ca *I–V* curve; and the function

R is derived from some electrodiffusion or barrier model of permeation through an ionic channel.

Although our own preliminary data indicate that a two-barrier model provides a better fit to the voltage-clamp data, for the present we shall make do with an electrodiffusion expression, since the exact form is not crucial for calculating the plateau, as long as the expression makes some sense for the case of zero internal Ca^{++}.

With the electrodiffusion form, the driving force function of Eq. 6 becomes:

$$R(V, [Ca^{++}]_i, [Ca^{++}]_o) = \frac{V\{1 - ([Ca^{++}]_i/[Ca^{++}]_o)\exp(V/12.5)\}}{[1 - \exp(V/12.5)]}. \quad (7)$$

The solutions shown in Fig. 3*d* are ones using this nonlinear expression for I_{Ca}, and in subsequent discussions of the all-Ca^{++} system the nonlinear form is assumed. Later, when we study the K^+ and Ca^{++} systems together, we revert to the linear approximation, because the voltage never leaves the linear region.

Let us return to a consideration of the phase planes of the individual conductance systems. By definition, the intersection points of two nullclines are equilibrium positions of V and μ, that is, singular points of Eqs. 3. The patterns of these singular points and the stability of the system in the neighborhood of each singular point can qualitatively explain the observed behavior.

For the all-K^+ system, each nullcline pair shown in Fig. 5*a* intersects only once, at a singular point which is stable ($\dot{V} = 0$ nullclines for several values of applied current are illustrated; the $\mu = 0$ nullcline does not change as I is varied). For the larger currents ($I = 100$, $I = 400$), the trajectories reach a voltage peak as they cross the $\dot{V} = 0$ nullcline. This represents the early peak seen in Fig. 2*b*; note that the peak occurs before V reaches its steady state and that the voltage then declines. Such behavior, sometimes referred to as a graded action potential, has been observed and discussed for synthetic systems having a single voltage-dependent conductance (Mueller and Rudin, 1967; Muller and Finkelstein, 1972).

Consider now the all-Ca^{++} system (Fig. 5*b*). There are three singular points in the phase plane for the value $I = 0$. Stability analysis shows that the points A and C are stable and that B is a saddle point. What happens when we go from $I = 0$ to, for example, $I = 100$? Because of the change in I, the system is described by a new $\dot{V} = 0$ nullcline, to the right of the original one, but the $\dot{M} = 0$ nullcline is not altered. The system now has only one singular point (C'), which is approached as the potential is depolarized under the influence of I (the trajectory for the depolarization is shown as a dotted line). This singular point is stable, representing a plateau voltage of the sort shown in Fig. 3*d*. What happens to the system when we return from $I = 100$ to $I = 0$? The initial conditions are now C' rather than A. The phase plane reverts to the original one with three singular points, including the saddle point, B. Saddle points always give rise to limiting curves called "separatrices," which cannot be crossed by phase trajectories. Thus, when the current is returned abruptly to zero, the system cannot cross the separatrix and return to the stable point, A. The only singular point available to the system is C, so that when the stimulus is turned off, the phase trajectory simply runs between C' and C, which leaves the system in a depolarized state. Thus, the observed persistence of the voltage plateau when the stimulus is turned off is a manifestation of bistability. Were an impulse of current used to raise instantaneously the voltage past the region where the separatrix

intersects the V-axis, bistability would be demonstrable in the $I = 0$ phase plane alone. Except for the use of a nonlinear term for the driving force, the behavior of the all-Ca^{++} system is exactly that of the theoretical V,m-reduced Hodgkin-Huxley equations devised by FitzHugh (1961) to explain threshold behavior in a qualitative way. FitzHugh's V,m-reduced system describes the discontinuous threshold behavior of a hypothetical system with a single activating conductance and no inactivation. The all-Ca^{++} barnacle fiber is a realization of this mathematical possibility.

Perturbations Caused by Ca^{++} Accumulation

The all-Ca^{++} version of Eq. 3 predicts stable plateau action potentials, but the real fiber does eventually repolarize. The mechanism directly responsible for repolarization has not been isolated. As it could be simple Ca^{++} accumulation or some form of slow inactivation, we now breifly describe in terms of the phase plane analysis how a slow process like Ca^{++} accumulation brings about repolarization. Accumulation of Ca^{++} intracellularly will simultaneously cause $\overset{*}{g}_{Ca}$ to decrease and $[Ca^{++}]_i$ to increase. To get a qualitative idea how this will affect the response, we need only look at the $\dot{V} = 0$ nullclines as we alter these two parameters (changes in these parameters do not change the $\dot{M} = 0$ nullcline since they do not appear in Eq. 4*b*). Note (Fig. 5*c*) that the upper stable point and the unstable point converge and then disappear as Ca^{++} accumulation proceeds (i.e., as $\overset{*}{g}_{ca}$ decreases and $[Ca^{++}]_i$ increases; the decrements and increments in these parameters are arbitrarily chosen). When the unstable point drops out, along with its separatrix, only one stable point remains and the system moves toward it, repolarizing as it does.

A more direct way to demonstrate the termination of the plateau is to include an equation for I_{Ca}-dependent intracellular Ca^{++} accumulation. We substitute the steady-state value of M_∞ for the term $M(t)$, since ion accumulation has very much slower kinetics than gating. The resultant differential equations are:

$$\frac{dV}{dt} = C^{-1}\{I - \overset{*}{g}_L(V - V_L) + \overset{*}{g}_{Ca}M_\infty(V)VR(V, [Ca^{++}]_i, [Ca^{++}]_o)\},$$

and

$$\frac{d[Ca^{++}]_i}{dt} \simeq K\{(CF)^{-1}\overset{*}{g}_{Ca}M_\infty(V)VR(V, [Ca^{++}]_i, [Ca^{++}]_o)\}. \quad (8)$$

Although the second equation is oversimplified (it does not take into account various sinks for intracellular Ca^{++}), it describes the major feature of accumulation. The value for the constant K was chosen to represent a Ca^{++}-accumulating compartment of 1 μm on the inner side of the membrane. Fig. 3*d* is the computed solution of Eqs. 8, which uses initial conditions that simulate the end of a stimulus pulse. After a gradual decline in voltage, there is a precipitous fall to rest. The actual mechanism for repolarization could be more complex than Ca^{++} accumulation, since Hagiwara and Nakajima (1966) have shown that Ca^{++} modulates the height of the Ca^{++} spike in a manner not consistent with simple changes in the driving force. As in some other Ca^{++}-excitable membranes (Eckert and Brehm, 1979), the Ca^{++} conductance in barnacle muscle may be inactivated by elevated $[Ca^{++}]_i$. Such a mechanism, however, would also be modelled, qualitatively, by concomitantly increasing $[Ca^{++}]_i$ and decreasing $\overset{*}{g}_{Ca}$.

Limit-cycle oscillations

The most interesting feature of the barnacle muscle behavior under current clamp is the voltage oscillation, which occurs only when the Ca^{++} and K^+ system are both operative. As different explanations have been adduced for the oscillations, we wish to explore how well the oscillations are explained by the two-conductance system itself with no additional mechanisms.

It can be shown (Fig. 6) that the V, M, N system of Eq. 1 predicts current-induced oscillations resembling the observed behavior. Numerical simulations, however, such as those of Fig. 6, require the simultaneous adjustment of several parameters, and it is not easy to learn the exact requirements for oscillation from numerical study of the full third-order system.

To study the oscillating state in some generality, we make use of the different relaxation times of the Ca^{++} and K^+ conductances. We study a reduced set of equations, in which the Ca^{++} system is assumed to be so much faster than the K^+ system that g_{Ca} is instantaneously in steady state at all times [i.e., $M = M_\infty(V)$]. For this approximation Eq. 1 becomes

$$I = C\frac{d\dot{V}}{dt} + g_L(V - V_L) + g_{Ca}M_\infty(V)\,(V - V_{Ca}) + g_kN(V - V_k),$$

and

$$\frac{d\dot{N}}{dt} = \lambda_N(V)\,(N_\infty(V) - N). \tag{9}$$

We shall call this the V,N reduced system, following the terminology of FitzHugh (1969). Eq. 9 describes a second-order system, whose properties can be visualized on the V,N-phase plane. It might be asked why we expect Eq. 9 to be a reasonable approximation to the full system. The justification lies in Tikhonov's theorem, utilized by Plant and Kim (1976; see their appendix). Eqs. 1 are of the proper form for the V and N differential equations to satisfy an

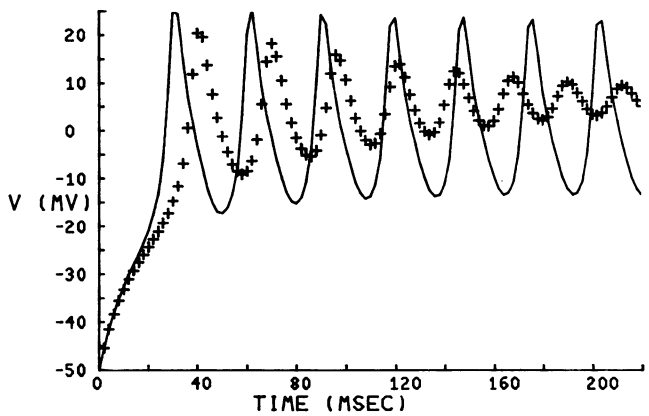

FIGURE 6 Examples of oscillations computed from the full V, M, N third-order system (Eq. 1). The parameters used for these computations are: $g_L = 2$, $V_L = -50$, $V_{Ca} = 100$, $V_K = -70$, $\bar{\lambda}_M = 1.0$, $\lambda_N = 0.1$, $V1 = 0$, $V2 = 15$, $V3 = 10$, $V4 = 10$, $C = 20$. The resting potential was taken to be -50 mV. For the broken line (+), $g_{Ca} = 6$ and $g_K = 12$, and for the solid line, $g_{Ca} = 4$ and $g_K = 8$. These figures are to be compared with the experimental data of Fig. 4. Voltage, V, mV; time, ms.

inequality of Tikhonov that allows reduction of the dimension of the phase space without changing the character of the singular point.

Under what conditions will the system defined by Eq. 9 have a stable limit cycle? The Poincaré-Bendixon theorem (Minorsky, 1962, p. 78; Pavlides, 1973, p. 7) states that if a phase trajectory remains in a finite domain of phase space for all time without approaching an equilibrium point, the trajectory is periodic or approaches a periodic trajectory.

To show that the solutions of Eqs. 9 remain in a finite domain of the V,N phase plane, we note that for both equations the derivatives of the dynamical variables change sign when the phase trajectory approaches the boundaries of a rectangle determined by the physical limits of the V and N variables. This is obvious for the N variable, which represents the fraction of open K^+ channels, and hence can vary only between 0 and 1. V, too, however, is bounded, for V cannot go beyond two limiting potentials, for which $\dot{V} = 0$:

$$V_{\min} = \frac{g_L V_L + g_K V_K + I}{g_L + g_K} < V < \frac{g_L V_L + g_{Ca} V_{Ca} + I}{g_L + g_{Ca}} = V_{\max}. \tag{10}$$

Since the trajectories are confined to this rectangle, it will be sufficient to find one unstable singular point in this region to ensure a stable limit cycle.

We next examine the character of the singular point for the reduced system. Fig. 7 shows the nullclines for Eqs. 9. The nullclines intersect once. The intersection point is given by $S = (V_s, N_s)$ such that:

$$N_s = N_\infty(V_s) = \frac{I - g_L(V_s - V_K) - g_{Ca} M_\infty(V_s)\,(V_s - V_{Ca})}{g_K(V_s - V_K)}. \tag{11}$$

In the usual fashion (Minorsky, 1962), Eqs. 9, when thought of as a general second order system of the form

$$\dot{V} = f_1(V,N), \quad \dot{N} = f_2(V,N), \tag{12}$$

will have stability properties determined by the character of the eigenvalues of the pair of equations linearized about the singular point, S. The eigenvalues (p), in turn, are the solutions of the characteristic equation:

$$p^2 - \left(\frac{\partial f_1}{\partial V} + \frac{\partial f_2}{\partial N}\right)_s p + \left(\frac{\partial f_1}{\partial V}\frac{\partial f_2}{\partial N} - \frac{\partial f_2}{\partial V}\frac{\partial f_1}{\partial N}\right)_s = 0. \tag{13}$$

In order to have a stable limit cycle, both roots must be positive if they are real or have a positive real part if they are complex. Since the first term in brackets in Eq. 13 is equal to the sum of the roots, and the second term in brackets is the product of the roots, the necessary condition for both roots positive is:

$$\left(\frac{\partial f_1}{\partial V} + \frac{\partial f_2}{\partial N}\right)_s > 0$$

$$\left(\frac{\partial f_1}{\partial V}\frac{\partial f_2}{\partial N} - \frac{\partial f_2}{\partial V}\frac{\partial f_1}{\partial N}\right)_s > 0. \tag{14}$$

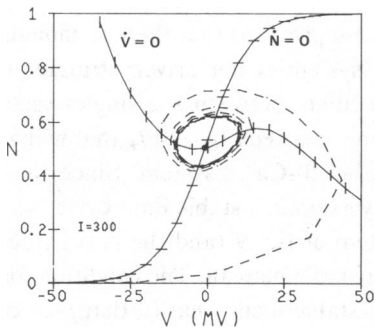

FIGURE 7

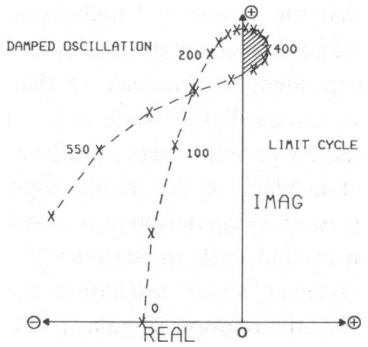

FIGURE 8

FIGURE 7 Nullclines in V, N that give a stable limit cycle. The nullclines are labeled; the spiral traces the trajectory of the system when I is changed from 0 to 300. The point at the intersection is an unstable node. Vertical and horizontal bars on the nullclines indicate the direction in which the trajectory must cross. Computations are based on the parameters used in Fig. 9, but with $I = 300$. The sufficient condition for oscillation is given by Eq. 15. Essentially, the condition states that the intersection must occur somewhere in the negative-resistance part of the Ca^{++} current-voltage curve. This is the ascending limb of the bump in the $\dot{V} = 0$ nullcline, as shown in the figure. An analogous condition for a somewhat different reduced system is given by Plant and Kim (1976). Voltage, V, mV.

FIGURE 8 Plot of real and imaginary parts of eigenvalue (p, in Eq. 13) of the linearized V, N-reduced equations as current is varied. The curve shown is the root with plus sign, the negative root leading to a mirror reflection (not shown) across the real axis. When the eigenvalues are real, they are represented by points on the real line. The shaded loop marks the range of current values for which the real part is positive, so that there is a stable limit cycle. The imaginary part of the eigenvalue is approximately equal to the oscillation frequency, so that the value on the imaginary axis shows the pattern of frequency variation with applied current. Parameters used in these computations are those of Fig. 9, but with I varied as indicated by the numbers adjacent to the curve.

The first inequality guarantees at least one positive root and the second guarantees that both roots have the same sign.

From Eq. 9 we can substitute the explicit expressions for the partial derivatives of Eq. 14, to obtain the following inequalities:

$$g_{Ca}\left(\frac{\partial M_\infty}{\partial V}\right)_s (V_{Ca} - V_s) > g_L + g_K N_s + g_{Ca} M_\infty(V_s) + C\lambda_N(V_s),$$

and

$$g_{Ca}\left(\frac{\partial M_\infty}{\partial V}\right)_s (V_{Ca} - V_s) < g_L + g_K N_s + g_{Ca} M_\infty(V_s) + g_K\left(\frac{\partial N_\infty}{\partial V}\right)_s (V_s - V_K). \qquad (15)$$

Eqs. 15 define the conditions on the various conductance parameters for a stable limit cycle. The inequalities can be given physical meaning if one notes that the term on the left hand side of Eqs. 15 is essentially proportional to the negative dynamic conductance contributed by the inward Ca current, and that the right hand side contains the term $\bar{g} = g_L + g_K N + g_{Ca} M$, which is the equivalent conductance at the operating point. Thus, Eqs. 15 can be rewritten as:

$$(\bar{g} + C\lambda_N)_s < \left[g_{Ca}\frac{\partial M_\infty}{\partial V}(V_{Ca} - V)\right]_s < \left[\bar{g} + g_K\frac{\partial N_\infty}{\partial V}(V - V_K)\right]_s, \qquad (16)$$

which says that the system will undergo a limit cycle oscillation, provided that the Ca^{++} negative resistance can overcome the losses, but also provided that there is enough restorative K^+ voltage-dependent conductance so that the system is not driven straight to the Ca^{++} plateau. Thus, the oscillatory state is an intermediate between the single-system extremes discussed earlier; to oscillate there must be a balance between I_{Ca} and I_K that will yield a single singular point in place of the saddle point of the all-Ca^{++} system. Since for values of I satisfying Eq. 16, this singular point is unstable, we obtain a stable limit cycle.

In addition to limit-cycle oscillations, the system of Eq. 9 (and the real barnacle muscle) can undergo damped "small" oscillations about a stable plateau. The condition for oscillatory transients is that the relevant singular point be a stable focus; that is, that p be complex and have a negative real part. From Eq. 13, the condition for complex roots is

$$\left(\frac{\partial f_1}{\partial V}+\frac{\partial f_2}{\partial N}\right)_s^2-4\left(\frac{\partial f_1}{\partial V}\frac{\partial f_2}{\partial N}-\frac{\partial f_2}{\partial V}\frac{\partial f_1}{\partial N}\right)_s<0. \tag{17}$$

Examination of the equivalent circuit for eq. 9 linearized about S shows that Eq. 17 is precisely the condition on the various reactance parameters of the equivalent parallel resonant circuit needed to get an underdamped response.

By studying how the eigenvalue, p, changes as experimental parameters are varied, we can see how the system goes through various forms of behavior. Fig. 8 shows how, as I is varied, there is a current interval for which the real part of p becomes positive. This is what is observed experimentally: the fiber begins to oscillate at some threshold of applied current and, eventually, as current is increased, the oscillations diminish in amplitude. For high Ca^{++} concentrations, the oscillations become nearly sinusoidal about a voltage near to the all-Ca^{++} plateau. Examples of how the oscillations change for various changes of parameters are shown in Figs. 9, 10, and 11. Fig. 9 shows the change as I is varied and the corresponding changes in the $\dot{V}=0$ nullcline. Fig. 10, in which g_{Ca}, g_K, g_L, λ_N, and N_∞ are varied substantially,

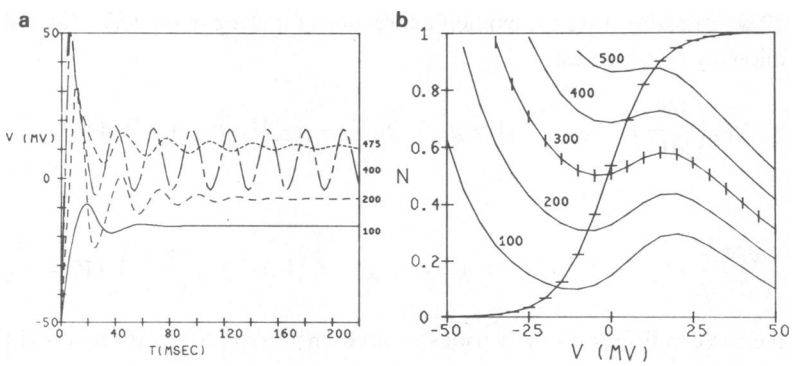

FIGURE 9 How system goes in and out of oscillation as current (I) is varied between 100 and 500. Parameters used are $g_L=2$, $g_{Ca}=4$, $g_K=8$, $V_L=-50$, $V_{Ca}=100$, $V_K=-70$, $\bar{\lambda}_M=0.1$, $\bar{\lambda}_N=1/15$, $V1=10$, $V2=-15$, $V3=-1$, $V4=14.5$, $C=20$. I is varied as indicated. (*a*) shows the voltage oscillations computed from the V, N-reduced system (Eq. 9). (*b*) shows the change in the $\dot{V}=0$ isocline as current is varied. Note by comparing with (*a*) that the range of stable oscillatory behavior coincides with the range of current for which the "negative resistance" portion of the $\dot{V}=0$ isocline intersects the $\dot{N}=0$ isocline. Voltage, V, mV; time, T, ms.

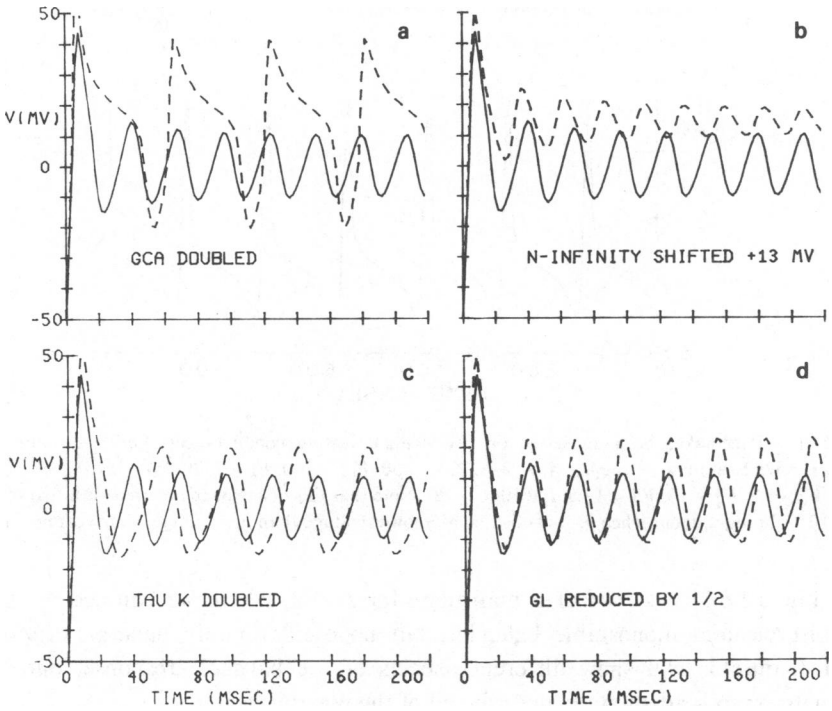

FIGURE 10 Effects of various parameter changes on the oscillation behavior. Although parameter changes alter the character of the oscillations, sustained oscillations occur over a wide range of parameters. In each graph the "control" solution (shown as a solid line) is that computed in Fig. 9 for $I = 300$. The dashed line is the solution after a single parameter change as indicated. (*a*) Increase in g_{Ca} ($g_{Ca} = 8$) changes shape of voltage oscillations from sinusoids to more rectangular spikes, and decreases the frequency. (*b*) A 13-mV depolarizing shift of the N_∞ ($V3 = 12$) curve increases the frequency of the oscillations and lowers the amplitude. (*c*) Increase in τ_K ($= \bar{\lambda}_N^{-1}$; $\bar{\lambda}_N = 1/30$) slows the oscillation, illustrating that the kinetics of g_K have a pronounced effect on the frequency. (*d*) Reducing leakage ($g_L = 1$) increases amplitude and introduces phase shift with little or no change in frequency. Voltage, mV; time, ms.

illustrates that the numerical requirements for oscillation are not stringent. Fig. 11 further illustrates this point, showing pacemaker-like oscillations obtained by changing the relative positions of M and N on the voltage axis.

Domains of Oscillatory Behavior

To give a fuller account of the type of variability encountered experimentally, we can assess the character of the singular point as different pairs of parameters are varied. Two-dimensional manifolds obtained by evaluating p from Eq. 13 give a qualitative map of system behavior and illustrate some of the phenomena which occur.

For example, Fig. 12 *a* shows how the system changes with varying g_{Ca} and g_K, with all other parameters held constant. In the figure we see a peninsula of oscillatory behavior when g_{Ca} and g_K are in more-or-less equal competition, as well as the other forms of behavior when one or the other conductance dominates. This particular map was done for a value of I that shows both types of oscillation but for which no combination of g_{Ca} and g_K can give bistable

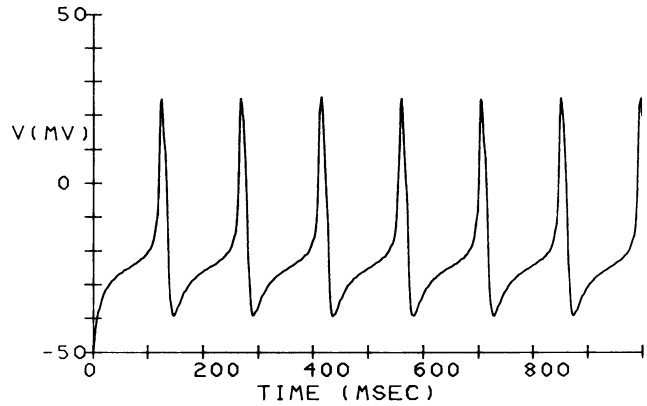

FIGURE 11 Pacemaker behavior based on two noninactivating conductances. For this solution the parameters were set to: $g_L = 2$, $g_{Ca} = 4$, $g_K = 8$, $V_L = -50$, $V_{Ca} = 100$. $V_K = -70$, $\bar{\lambda}_M = 0.1$, $\bar{\lambda}_N = 1/15$, $V1 = -1$, $V2 = 15$, $V3 = 10$, $V4 = 14.5$, $I = 50$, $C = 20$. Note that this behavior (compared with that of Figs. 9 and 10) is brought about when g_{Ca} is activated at a lower voltage than g_K. Voltage, V, mV; time, ms.

behavior. Fig. 12 *b* shows part of a map done for $I = 0$, where we can see the boundary between bistable and monostable behavior, but no oscillation. In general, different two-parameter manifolds will show different aspects of the barnacle response, but no single two-parameter map is adequate to describe all of the possibilities.

One use for the two-parameter manifolds is to illustrate qualitatively some of the

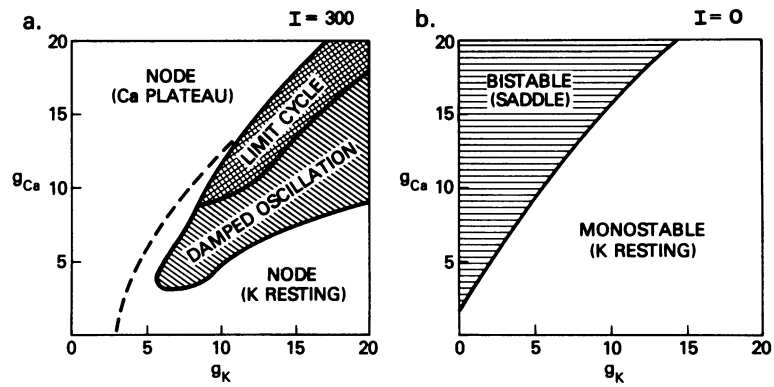

FIGURE 12 Parameter manifolds showing character of singular point for different combinations of g_{Ca} and g_K. Except for varying g_{Ca}, g_K, and I, the parameters used are those of Fig. 9. (*a*) $I = 300$. For this value of stimulating current the system can either be monostable as in the unshaded regions, or show oscillatory behavior, as in the shaded regions. Stable (limit cycle) oscillations occur only for the combinations of g_{Ca} and g_K that give an unstable equilibrium point. All such values fall in the crosshatched region. In the lower shaded region, the singular points are complex but have negative real parts; hence, the system has an oscillatory response to current transients, which then decays to a steady voltage. The unshaded regions have single equilibrium points which are stable nodes. (*b*) $I = 0$. With no injected current the system cannot oscillate. When g_{Ca} and g_K are varied, the two-parameter manifold divides into two regions. The unshaded region represents single stable nodes, whereas any combination in the shaded half-plane has three singular points, constituting two stable nodes and a saddle point, and therefore can exhibit bistable behavior.

phenomena which can occur when a slow variable, such as Ca^{++} accumulation, comes into play. One might expect a slow change to act as a secular perturbation bringing the system across the boundaries between two regions on a parameter map. Thus, a system with high external Ca^{++} might show oscillatory behavior near the all-Ca^{++} plateau until the Ca^{++} buildup knocks the system out of oscillation. Such a set of double relaxation oscillations is shown experimentally in Fig. 4*cvi*. This behavior is clearly too complicated for the approximate phase plane system, but the maps give a hint as to what might be happening.

DISCUSSION

This analysis was motivated by a wish to explore the variable behavior originating for a simple system of two noninactivating gated conductances. Our results indicate that a good part of the oscillatory voltage behavior of EGTA-perfused barnacle muscle can be anticipated from the two noninactivating conductances, without recourse to more complex conductance systems. Two important features of the simple system are that oscillatory solutions occur over a relatively wide region of the parameter space and that the character of the oscillations varies through this space. This coincides nicely with the barnacle fiber which displays variable oscillations (some sustained, some damped) and has extremely variable conductance magnitudes (see e.g., Keynes et al., 1973). The first feature—that the parameter requirements for oscillation are not rigorous—is fortunate, because parameters like the time and voltage dependence of the excitability mechanisms in barnacle are either poorly known or not agreed upon by different workers. Because numerical requirements for oscillations proved not to be tightly restricted, the generality of the model is enhanced.

Two modes of oscillation are produced by the system: damped oscillations and sustained or limit cycle oscillations. The barnacle apparently produces both kinds, although it is difficult, with a finite stimulating pulse, to distinguish between slowly damping oscillations and sustained ones. A point worth noting is the manner in which solutions may change in character as a parameter is monotonically varied. We illustrated a case for varying current in which the system went in turn from no oscillations to damped oscillations, to limit-cycle oscillations, to damped oscillation, and, finally, back again to no oscillations. This example should emphasize the complexity of behavior inherent in this mechanistically simple system.

There are, clearly, aspects of barnacle fiber voltage behavior which are not encompassed by the two conductance, perfect space-clamp model we have used. It cannot, for example, produce the sort of oscillations that start small and grow, or the bistable oscillation pattern. Nor can it produce the amplitude-modulated oscillations that are occasionally seen. It is not clear whether these phenomena result from artifacts (e.g., "patchiness" in the membrane due to injury, or failure of radial space clamp) or from processes like ion accumulation or additional conductances. Where it is desired to investigate higher order effects without adding further equations, graphical analysis is more useful for exploring various possibilities. We have illustrated this for the simple example of the possible role of Ca^{++} accumulation in the plateau action potential. Parameter manifolds can be used to examine variation of two parameters simultaneously.

A virtue of the stability analysis is that one can vary parameters and use the eigenvalues to predict the nature of the voltage behavior without the necessity of integrating the differential equations. This approach may prove useful in analyzing aspects of the behavior of other

systems of a similar nature, such as dendritic calcium spikes of pyramidal cells (Llinas, 1979) or the slow voltage oscillations of cells that have states dominated by a g_{Ca} and a calcium-mediated potassium conductance.

As an example of the latter type of system, pancreatic β-cells stimulated with glucose and treated with high concentrations of TEA produce sustained trains of spikes (Atwater et al., 1979*c*), and it seems that the major excitability mechanisms under these conditions are a g_{Ca}- and a $[Ca^{++}]_i$-activated g_K (Atwater et al., 1979*a*; Atwater et al., 1979*b*). Likewise, neuroblastoma cells produce oscillations dependent on a g_{Ca}- and a Ca^{++}-dependent, quinine-sensitive g_K (Fishman and Spector, 1980). In both these cell types, multiple conductance mechanisms, which cannot necessarily be fully blocked pharmacologically, complicate the interpretation of results. Moreover, the β-pancreatic cell, due to its small size, is not amenable to voltage-clamp analysis. In order to assess the possible significance of interactions of g_{Ca} and $[Ca^{++}]$-activated g_K, it would be worthwhile to explore, qualitatively, the range of behavior predictable on the basis of the two Ca^{++}-dependent mechanisms.

The authors would like to thank Dr. D. L. Gilbert for his aid and instruction during the early stages of the experimental work. We also wish to thank Dr. G. Ehrenstein, R. FitzHugh, and T. G. Smith for their comments on the manuscript.

Received for publication 29 July 1980 and in revised form 26 November 1980.

REFERENCES

Atwater, I., C. M. Dawson, B. Ribalet, and E. Rojas. 1979*a*. Potassium permeability activated by intracellular calcium ion concentration in the pancreatic β-cell. *J. Physiol (Lond.)* 288:575–588.

Atwater, I., G. T. Eddlestone, B. Ribalet, and E. Rojas. 1979*b*. Calcium channel voltage noise across the beta-cell membrane in islet of Langerhans of mouse. *J. Physiol. (Lond.)* 291:69P–70P.

Atwater, I., B. Ribalet, and E. Rojas. 1979*c*. Mouse pancreatic β-cells: tetraethylammonium blockage of the potassium permeability increase induced by depolarization. *J. Physiol. (Lond.)* 288:561–574.

Beirao, P. S., and N. Lakshminarayanaiah. 1979. Calcium carrying system in the giant muscle fibre of the barnacle species, *Balanus nubilus*. *J. Physiol. (Lond.)* 293:319–327.

Eckert, R., and P. Brehm. 1979. Ionic mechanisms of excitation in *Paramecium*. *Annu. Rev. Biophys. Bioeng.* 8:353–383.

Ehrenstein, G., and H. Lecar. 1977. Electrically gated ionic channels in lipid bilayers. *Q. Rev. Biophys.* 10:1–34.

Fishman, M. C., and I. Spector. 1980. Blockage of a calcium-dependent potassium conductance in neuroblastoma cells by quinine. *J. Supramol. Struct.*, Suppl. 4:83.

FitzHugh, R. 1961. Impulses and physiological states in theoretical models of nerve membrane. *Biophys. J.* 1:445–466.

FitzHugh, R. 1969. Mathematical models of excitation and propagation in nerve. *In* Biological Engineering. H. P. Schwann, editor, McGraw-Hill Publications, New York.

Hagiwara, S., J. Fukuda, and D. C. Eaton. 1974. Membrane currents carried by Ca, Sr, and Ba in barnacle muscle fiber during voltage clamp. *J. Gen. Physiol.* 63:564–578.

Hagiwara, S., H. Hayashi, and K. Takahashi. 1969. Calcium and potassium currents of the membrane of a barnacle muscle fibre in relation to the calcium spike. *J. Physiol. (Lond.)* 205:115–129.

Hagiwara, S., and S. Nakajima. 1966. Effects of the intracellular Ca ion concentration upon excitability of the muscle fiber membrane of a barnacle. *J. Gen. Physiol.* 49:807–818.

Hagiwara, S., and S. Nakajima. 1966. Differences in Na and Ca spikes as examined by application of tetrodotoxin, procaine, and manganese ions. *J. Gen. Physiol.* 49:793–806.

Hencek, M., and J. Zachar. 1977. Calcium currents and conductances in the muscle membrane of the crayfish. *J. Physiol. (Lond.)* 268:51–71.

Hodgkin, A. L., and A. F. Huxley. 1952. A quantitative description of membrane current and its application to conduction and excitation in nerve. *J. Physiol. (Lond.)* 117:500–544.

Keynes, R. D., E. Rojas, R. E. Taylor, and J. Vergara. 1973. Calcium and potassium systems of a giant barnacle muscle fibre under membrane potential control. *J. Physiol. (Lond.)* 229:409–455.

Knott, G. 1979. MLAB: An On-line Modeling Laboratory. 8th edition. Division of Computer Research and Technology, National Institutes of Health (NIH), Bethesda, Md.

Lecar, H., G. Ehrenstein, and R. Latorre. 1975. Mechanism for channel gating in excitable bilayers. *Ann. N.Y. Acad. Sci.* 264:304–313.

Lecar, H., and R. Nossal. 1971. Theory of threshold fluctuations in nerves. I. Relationships between electrical noise and fluctuations in axon firing. *Biophys. J.* 11:1048–1067.

Llinas, R. 1979. The role of calcium in neuronal function. *In* The Neurosciences, Fourth Study Program. F.O. Schmitt and F.G. Worden, editors. MIT Press, Cambridge, Mass. 555–571.

Minorsky, N. 1962. Introduction to non-linear oscillators. D. Van Nostrand Co., New York.

Mounier, Y., and G. Vassort. 1975. Evidence for a transient potassium membrane current dependent on calcium influx in crab muscle fibre. *J. Physiol. (Lond.)* 251:609–625.

Mueller, P., and D. O. Rudin. 1967. Action potential phenomena in experimental bimolecular lipid membranes. *Nature (Lond.)* 213:603–604.

Muller, R. V., and A. Finkelstein. 1972. Voltage-dependent conductance induced in thin lipid membranes by monazomycin. *J. Gen. Physiol.* 60:263–284.

Murayama, K., and N. Lakshminarayanaiah. 1977. Some electrical properties of the membrane of the barnacle muscle fibers under internal perfusion. *J. Membr. Biol.* 35:257–283.

Pavlides, T. 1973. Biological oscillators: their mathematical analysis. Academic Press, Inc., New York.

Plant, R. E. 1976. The effects of Ca^{++} on bursting neurons: a modelling study. *Biophys. J.* 21:217–237.

Plant, R. E., and M. Kim. 1976. Mathematical description of a bursting pacemaker neuron by a modification of the Hodgkin-Huxley equations. *Biophys. J.* 16:227–244.